

Electrical resistivity anomalies offshore a carbonate coastline: Evidence for freshened groundwater?

Amir Haroon¹, Aaron Micallef^{1,2}, Marion Jegen¹, Katrin Schwalenberg³, Jens Karstens¹, Christian Berndt¹, Xavier Garcia⁴, Michel Kuehn¹, Enzo Rizzo⁵, Nicoletta Chiara Fusi⁶, Chibuzo Valeria Ahaneku^{2,7}, Lorenzo Petronio⁸, Zahra Faghieh¹, Bradley A. Weymer¹, Michele De Biase⁹, Francesco Chidichimo⁹

¹ Helmholtz Centre for Ocean Research, GEOMAR, Kiel, Germany

² Marine Geology & Seafloor Surveying, Department of Geosciences, University of Malta, Malta

³ Federal Institute for Geosciences and Natural Resources (BGR), Germany

⁴ Institute of Marine Sciences, CSIC, Barcelona, Spain

⁵ Dipartimento di Fisica e Scienze della Terra, University of Ferrara, Ferrara, Italy

⁶ Earth and Environmental Sciences Department, University of Milano-Bicocca, Italy

⁷ Department of Geological Sciences, Nnamdi Azikiwe University, Awka, Anambra State, Nigeria

⁸ Istituto Nazionale di Oceanografia e di Geofisica Sperimentale (OGS), Trieste, Italy

⁹ Department of Environmental Engineering, University of Calabria, Rende, Italy

* Correspondence to A.M. (amicallef@geomar.de)

ORCID IDS:

Amir Haroon 0000-0001-5138-6730

Aaron Micallef 0000-0002-9330-0648

Marion Jegen 0000-0001-6307-8428

Katrin Schwalenberg 0000-0002-0511-6075

Jens Karstens 0000-0002-9434-2479

Christian Berndt 0000-0001-5055-0180

Xavier Garcia 0000-0002-8500-4224

Michel Kuehn 0000-0002-6323-896X

Enzo Rizzo 0000-0003-4630-2365

Nicoletta Chiara Fusi

Chibuzo Ahaneku Valeria 0000-0002-6479-4853

Lorenzo Petronio 0000-0003-1762-9166

Zahra Faghieh 0000-0002-6751-8934

Bradley A. Weymer 0000-0003-3762-8056

Michele De Biase 0000-0003-2564-3283

Francesco Chidichimo 0000-0003-4892-1987

Words:

Abstract: 149 (with Title)

Introduction: 465 (w Title)

Strat. Framework: 218 (w Title)

Data & Results: 1269 (w Title)

Discussion: 1013 (w Title)

Conclusions: 256 (w Title)

Acknowledgements: 158 (w Title)

Total: 3528

3 Figures, 1 Table

This article has been accepted for publication and undergone full peer review but has not been through the copyediting, typesetting, pagination and proofreading process, which may lead to differences between this version and the [Version of Record](#). Please cite this article as [doi: 10.1029/2020GL091909](#).

This article is protected by copyright. All rights reserved.

Abstract

Carbonate lithologies host considerable quantities of the Earth's freshwater resources and partially supply a quarter of the global population with drinkable water. Carbonates constitute substantial amounts of the global coastlines, yet it is not known if and how they can sustain freshened groundwater offshore. Here, we use controlled source electromagnetic, seismic reflection, and core sample data to derive a lithological model for the eastern margin of the Maltese Islands and identify four distinct resistivity anomalies within the Upper Coralline Limestone, Globigerina Limestone, and Blue Clay formations. The anomalies hosted in the former are likely associated to low porosities, whereas the anomaly within the latter is indicative of pore fluid freshening. Hydrogeological modeling suggests that freshened pore fluids, emplaced during sea-level lowstands and preserved in low permeability units, are potentially still found within carbonate shelves. However, resource potential is low due to its relict nature and low permeability host environment.

Plain language summary

Coastal regions with freshened groundwater beneath the seafloor are found worldwide. Here we report on a geophysical study conducted off the eastern coastline of the Maltese Islands where a number of resistivity anomalies are observed in limestones. The anomalies located offshore southeast Malta are likely associated to freshened groundwater. Hydrogeological modeling suggests that this groundwater was deposited during lower sea levels and preserved in fine grained units. Our study indicates that offshore freshened groundwater may be found offshore limestone coastline in dry climates, but its potential to be used as a source of freshwater is likely low.

Key points

- Geophysical data and hydrogeological modeling are applied to detect offshore freshened groundwater in a semi-arid carbonate setting
- Globigerina Limestone and Blue Clay located offshore SE Malta likely host a disconnected offshore freshened groundwater body
- The resistive anomalies within the Upper Coralline Limestone are interpreted as localized porosity variations.

- This OFG was emplaced during sea-level lowstands and preserved in low permeability units

Introduction

Groundwater resources in coastal regions are globally deteriorating due to population growth, pollution, and climate change (Aeshbach-Hertig & Gleeson, 2012; Richey et al., 2015; Michael et al. 2017). Problems are especially critical in arid regions, where groundwater is often the only source of freshwater, and where periods of highest consumption coincide with periods of lowest meteoric recharge. To mitigate the increasing demand on groundwater systems, offshore freshened groundwater (OFG) has been proposed as an alternative source of potable water (Bakken et al., 2012). The key emplacement mechanisms for OFG include present-day meteoric recharge from the onshore portion of the aquifer (Michael et al., 2016, Paldor et al., 2020) and/or meteoric recharge of shelf areas that were exposed during sea-level lowstands (Meisler et al., 1984). In the case of the latter, emplaced groundwater migrated landwards more slowly than the ensuing sea-level rise, and remnants of these groundwater bodies are still found offshore (Harrar et al., 2001; Person et al., 2003; Cronin, 2012; Post et al., 2013). OFG systems today are either recharging through an active connection to their terrestrial counterparts, or disconnected, relict systems. In both cases, the characteristics of OFG are poorly constrained, and questions regarding their geometry and distribution, as well as the geological controls and timing of emplacement remain unanswered (Micallef et al., 2021).

Several studies have demonstrated the effectiveness of controlled source electromagnetic (CSEM) methods to image the electrical resistivity distributions associated with OFG along continental margins and volcanic islands (e.g. Haroon et al., 2018a Gustafson et al., 2019; Attias et al., 2020; Micallef et al., 2020; Attias et al., 2021). The bulk electrical resistivity is sensitive to both changes in pore fluid salinity and sediment matrix porosity (Archie, 1942). Therefore, integrative analyses of CSEM with multi-channel seismic (MCS) reflection data (e.g. Bertoni et al. 2020) have proven effective in differentiating lithological units from pore fluid salinity anomalies in siliciclastic margins (e.g. Gustafson et al., 2019). In comparison, freshened groundwater within carbonate margins has rarely been investigated using CSEM and MCS (one of the few studies was presented by Evans & Lizarralde, 2011) and their hydrogeology remains poorly constrained. This is an important gap in knowledge, considering that carbonates represent major aquifers (Laugié et al. 2019), comprise approximately 16% of the global coastline excluding Antarctica (Goldscheider et al. 2020), and outcrop along >15% of the Mediterranean catchment area (Margat, 1998; Bakalowicz, 2015).

In this study we combine CSEM, MCS, and lithological data with numerical hydrogeological modeling to map freshened groundwater offshore the Maltese Islands and to identify the factors governing its emplacement and understand its resource potential. This archipelago has a semi-arid climate and one of the lowest ratios of water resources per inhabitant globally (FAO, 2006), motivating the exploration for unconventional water resources using a combined geophysical, geological, and hydrogeological approach.

Stratigraphic Framework

The Maltese Islands are located in the central part of the carbonate Pelagian Platform (Figure 1). An Oligo-Miocene sedimentary succession of four formations is exposed across the archipelago (Pedley et al., 1976): Lower Coralline Limestone (LCL), Globigerina Limestone (GL), Blue Clay (BC), and Upper Coralline Limestone (UCL); the limestone formations are further subdivided into members (Oil Exploration Directorate, 1993).

Three types of meteorically recharged groundwater bodies are hosted within the carbonate lithologies onshore. The largest groundwater body is hosted within the LCL and GL formations and comprises a freshwater Ghyben-Herzberg lens floating above saltwater (Bakalowicz & Mangion, 2003). It provides the primary source of potable water in Malta and has a residence time of 15-40 years (Stuart et al., 2010). The other two groundwater bodies have been identified from onshore drilling within the UCL and are either perched over the impermeable BC formation above sea-level, or in valleys below sea-level (ERA, 2015). Onshore recharge of all groundwater bodies is equivalent to ~25% of the annual precipitation of 550 mm (FAO, 2006; Galdies, 2013).

Our study area is located offshore the eastern coast of the Maltese Islands (Figure 1). The seafloor predominantly consists of gently sloping terrain and represents a submerged paleo-landscape (Micallef et al., 2013) the boundary of which is delineated by fault escarpments, paleo-shorelines and shore platforms.

Methods and Results

Physical property measurements

Seven core samples were collected at two sites on Malta and Gozo in 2018 (blue markers in Figure 1). They represent lithological members that most commonly outcrop across the islands (cf. Table 1). The samples were analyzed in terms of porosity, density, hydraulic conductivity, and electrical resistivity to define plausible ranges for interpreting geophysical and

hydrogeological models. Additionally, Table 1 lists reported literature data along with P-wave velocities and unit thicknesses measured at borehole BH3 (pink marker in Figure 1a).

Resistivities measured on samples saturated with seawater (0.2 Ωm) range between 1.96 and 4.43 Ωm and tend to increase with stratigraphic age of the corresponding unit. Measured porosities lie within the broad ranges found in literature. Higher P-wave velocities are measured for the UCL and LCL formations compared to the Globigerina members. This stands in agreement with a positive density correlation, but departs from the inverse correlation of the formation porosities.

Geophysical methods and results

Five 2D multi-channel seismic (MCS) lines (labelled 2, 4, 5, 6 and 9 in Figure 1) were acquired in October 2018 using a single mini-GI gun source with a Geometrics Geo-eel solid state streamer consisting of four 12.5 m long sections. Data processing included streamer geometry correction, seismic trace balancing, bandpass-filtering, NMO-correction, and 2D-Stolt-migration using a seismic velocity of 1500 m/s.

Table 1: Physical properties of the outcropping lithologies on the Maltese Islands. Literature values are marked by footnotes (1: Stuart et al. (2010); 2: Cassar (2010); 3: Cooke et al. (2018); 4: Bakalowicz & Mangion (2003); 5: Sapiano et al. (2017a, b); 6: ERA (2015)) and combined with measured data obtained from core samples (porosity, hydraulic conductivity, density, resistivity) and P-wave velocities measured within borehole BH3 using a three-component geophone and hydrophone streamer with an offset of 10.6 m. UCL-T and LCL-X are incomplete due to insufficient saturation during laboratory measurements indicating low permeability. Computed porosities derived from the ratio of saturated water volume to sample volume coincide well with literature values, whereas measured hydraulic conductivities are several orders of magnitude smaller. Literature values were largely derived from pump tests in the field, whereas our values are from small-scale lab measurements, which may explain the above-mentioned differences. Data descriptions are displayed in Figures S1-S3 of the SI.

Formation	Member	Porosity		Hydraulic Conductivity (m/s)		P-Wave Velocity (m/s)		Thickness at BH3 (m)	Density (g/cm ³)	Resistivity (Ωm) seawater saturated
		Literature ^{1,2,3}	Measured	Literature ^{4,5,6}	Measured					
Upper Coralline	Tal-Pitkal (UCL-T)	0.02 - 0.45	-	$10^{-5} - 10^{-8}$	-	2741	20.5	2.60	1.77	1.96
	Mtarfa (UCL-M)		0.3		5.0×10^{-7}					
Blue Clay	BC	0.35	-	10^{-8}	5.90×10^{-11}	1700	52	1.87	-	-
Globigerina (GL)	Upper (UGL)	0.24 - 0.41	0.36	$8 - 9.95 \times 10^{-6}$	4.0×10^{-9}	2113	2066	8	1.53	2.27
	Middle (MGL)		0.29		8.30×10^{-10}	1993		11	1.65	2.38
	Lower (LGL)		0.27		1.68×10^{-8}	2335		6	1.79	2.68
Lower Coralline (LCL)	Xlendi (LCL-X)	0.02 - 0.3	-	$0.2 - 9.95 \times 10^{-4}$	-	2957	79	2.54	-	-
	Attard (LCL-A)	0.02 - 0.28	0.19		7.28×10^{-8}			2.09	4.43	4.43

1: Stuart et al (2010); 2: Cassar (2010); 3: Cooke et al. (2018); 4: Bakalowicz & Mangion (2003) 5: Sapiano et al. (2017a,b) 6: ERA (2015).

During the same cruise, a seafloor-towed CSEM experiment was carried out using a modular, electric dipole-dipole system consisting of a 100 m long transmitter dipole followed by three inline receivers at offsets of 150 m, 280 m, and 510 m, respectively (Figure S4 in SI and Schwalenberg et al., 2017). Data were acquired along five profiles labelled lines 2, 5, 6, 8, and 9 in Figures 1 and 2. Following the shallow-water sensitivity considerations of Haroon et al. (2020), only step-on data were processed at stationary waypoints marked by black triangles in Figure 2. Data errors are quantified by stacking repeated step functions at each waypoint resulting in a time-dependent noise model that varied each day of the survey and also for each receiver (presumably due to electrode noise). Overall, the source-normalized absolute noise floor is quantifiable at $5e^{-12}$ V/m at 1 s. Additionally, a 5% minimum relative error floor is assigned to account for systematic distortions due to imprecise navigation data of the seafloor-towed system. The processed CSEM data were interpreted using isotropic models in the time-domain using MARE2DEM (Key, 2016; Haroon et al., 2018b). Data fits for each profile are presented in Figures S5-S10 of the SI. Note that vertical transverse isotropic models lead to consistent results (see Figures S11 and -S12 of the SI) and, therefore, anisotropy was not considered in this study.

Due to the strong reflectivity of the carbonate seafloor, only limited seismic energy penetrated the sub-seafloor, restricting lithological inferences based on seismic data alone (Figure S14 of SI). Thus, seismic interpretations along lines 2, 5, 6, and 8 were supported by borehole data from BH3, morphological observations, CSEM resistivity models, and in-situ data from remotely operated vehicle (ROV) imagery. Lithological inferences are traced above the electrical resistivity models in Figure 2. Along line 9, seismic data had higher quality and was correlated with Gatt (2012), who shows a >60 m thick GL formation with strata tilted 4° overlying LCL.

The derived geological models are jointly-interpreted with the electrical resistivity models and core samples to identify anomalous features indicating lithological boundaries, local porosity anomalies, or OFG occurrences. The inferred offshore geology displayed in Figure 2 shows an overburden layer consisting of marl, gravel, and sand, which generally comprises a mixture of hemipelagic and lowstand deposits. Below, a sequence of UCL, BC, GL, and LCL of varying thicknesses exists. ROV imagery and samples collected at the base of the escarpment show outcrops of LCL (Figure 2b). Box canyons, known to occur only within the UCL formation onshore, are visible at the top of the escarpment (Figure 1), suggesting that UCL comprises the upper part of the escarpment.

All 2D resistivity models in Figure 2 achieve a target misfit of $RMS=1$ and overlay the interpreted lithology. The corresponding error models and data fits are found in Figures S5-S10 of the SI. The overburden is represented by a conductor of $\sim 1 \Omega m$ (labelled C1 where corresponding to channel infill). Along lines 2, 5, 6, and 8 (Figure 2b-e), a prominent conductive feature ($\sim 1 \Omega m$) is also located at a depth of $\sim 100 m$, which corresponds to the BC formation. Above the BC, UCL appears as a more resistive unit ($2-4 \Omega m$) that contains local resistivity anomalies ($>6 \Omega m$). On line 8, a $\sim 50 m$ thick resistor of $14 \Omega m$ (R2) is located within UCL towards the SE of the paleo-channel (labelled C3, Figure 2d). On line 6 (Figure 2e), an anomalous high resistor R1 ($>15 \Omega m$) is observed within UCL near the seafloor at 3800 m. Line 5 (Figure 2c) shows a dipping resistive structure R3 ($\sim 6 \Omega m$) within UCL between 0 – 2000 m below a NW-SE oriented graben (Illies, 1981). Across the northern half of the study area (Lines 2, 5, 6, and 8), GL and LCL feature below the BC as a deep-lying resistor ($>8 \Omega m$). However, the interface between BC and this resistor is poorly defined due to the limited vertical resolution of unconstrained CSEM inversion and a lack of adequate seismic reflection data. Along line 9 (Figure 2a), tilted strata appear as a resistive structure ($6-10 \Omega m$) underlying a conductive fine sand to muddy sediment layer. A local resistivity anomaly of $\sim 10 \Omega m$ (labelled R4) lies within GL at a depth of 40 – 50 m below the seafloor and is bounded below and towards the coast by conductor C2 ($1-2 \Omega m$). At depths $>300 m$, the deep-lying resistor is associated with LCL.

Hydrogeological modeling

A shore-normal cross-sectional hydrological model of groundwater flow and solute transport was constructed along line 9 based on the above-mentioned observations (Figure 3b). A scenario in which sea-level is gradually increased from -130 m to 0 over the past 20 ka was considered to assess how OFG emplaced during the Last Glacial Maximum responds to salinization. The aquifer is considered as unconfined and each geological formation is modeled as homogeneous. No layers of impermeable material are located both above and below the aquifer. The water table is at atmospheric pressure, and thus is able to rise and fall depending on external forcing. Three different hydraulic-conductivity anisotropy factors (K_h/K_v of 1, 10 and 100) are investigated to assess their influence on OFG evolution. The present-day result from the model simulation that is most comparable to the geophysical inversion model is shown in Figure 3b and corresponds to an anisotropy factor of 100. Such an anisotropy is justified for the geological setting and scale we are modeling; anisotropies of numerical models lumping multiple geological layers into a single hydrostratigraphy over km scales can go up to 1000-

10000, especially for sedimentary rocks (Freeze and Cherry, 1979). Detailed descriptions regarding the hydrogeological modelling is listed in Section S6 and Figures S15-S19 of the SI.

In this scenario, OFG occurs as a 1 km extension of the terrestrial groundwater system within LCL (-2000 to 0 m), and as an isolated groundwater body (2500 to 5000 m), predominantly hosted in the low-permeability BC and GL formations. The evolution from the initial freshwater conditions to this final result entails a progressive salinization with the isolated OFG preserved in the lower permeability units (Figure S19 in SI). The salinization is slower than the sea-level rise. A decrease in anisotropy results in an increase in the overall salinity of the groundwater and a reduction in its offshore extent (Figures S17-S19 in SI).

Discussion

CSEM resistivity models reveal complex internal architectures in the UCL and GL formations, comprising of local resistivity anomalies within a background resistivity range between 2-4 Ωm . Assuming Archie's relationship (Archie, 1942) for fully-saturated carbonate rock (Glover, 2016),

$$\rho = \Phi^{-m} \rho_w \quad (1)$$

a distinct increase of bulk resistivity (ρ) is either caused by a porosity (Φ) decrease, a cementation exponent (m) increase, or a porewater resistivity (ρ_w) increase. The latter is proportional to a salinity decrease (Figure 3a). Note that a cementation increase alone is rather unlikely to cause the localized resistivity variations we observe for R1-R4, whereas variations in porosity and salinity can easily account for the observed resistivity variations (cf. panels of Figure 3a).

Using the reported UCL and GL porosities (cf. Table 1), and assuming a cementation exponent of $m=1.8$ (Figure S3 of SI), we can estimate that seawater-saturated (38 PSU) GL resistivities lie between 1-3 Ωm , and between 1.5 and several hundred Ωm for UCL. Note that this upper limit is due to the extremely low porosity of 0.02 reported in one published study (Cassar, 2010).

The background resistivities for UCL observed along lines 2, 5, 6 and 8 indicate a porous seawater-saturated carbonate matrix, with local resistivity variations that can range between 6-15 Ωm (i.e. anomalies R1-R3). R1 (>15 Ωm) is located at the seafloor within UCL along line 6 (Figure 2e). R3 on line 5 (Figure 2c) is interpreted as dipping UCL strata at an inferred graben

structure (Illies, 1981). The observed resistivities are 2-5 times larger than the background seawater-saturated UCL resistivities along lines 5 and 6. Both R1 and R3 extend to the seafloor, yet no freshened groundwater discharge was registered by the CTD (conductivity, temperature, depth) sensor (mounted on the CSEM system) and pore water sampling from gravity cores (Berndt et al., 2021). These observations, together with a lack of a confining unit above the resistivity anomalies, suggest that the latter are unlikely to be associated with OFG. Along line 8 (Figure 2d), R2 is embedded in the UCL formation at several tens of meters depth below seafloor to the east of Gozo. Here, an OFG system with local pore fluid freshening is a more plausible scenario, with the permeable UCL interbedded between less permeable confining units above and below. However, similar to anomalies R1 and R3, R2 can also be explained by a local decrease in the porosity, which in UCL can be attributed to the occurrence of UCL-T. Resistivity anomaly R4 on line 9 (Figure 2a) is found within GL, which exhibits lower variability in porosity compared to UCL. Thus, R4 is indicative of a salinity anomaly rather than a localized porosity decrease. It extends <1 km along the profile and is overlain by BC and muddy sands, which act as confining units. The porosities of GL and BC lie above 0.24 and 0.35 respectively, implying that local pore water salinity values could be between 3.5-10 PSU (converted with the porosity range in Table 1 and Figure 3a). The numerical simulations demonstrate that the geological setting along line 9 is conducive to the emplacement of OFG (Figure 3b), and that the model-derived salinity pattern qualitatively compares with the CSEM inversion model (Figure 3c). The present-day OFG in the hydrogeological simulation occurs as a disconnected body, although it also includes a smaller 1 km extension of the terrestrial groundwater system that was not covered by the CSEM survey. The model simulations suggest that the OFG was emplaced during previous sea-level lowstands, when the offshore geological formations were charged with freshwater by enhanced topographically-driven flow and infiltration. As sea-level rose, the freshwater was better preserved in GL and BC due to their low permeability (Figure S19). The disconnection between the OFG body and the terrestrial groundwater system at present is due to salinization of the more permeable intervening units and the thin GL formation (cf. Figure S19). The modeling results suggest that active meteoric recharge from onshore does not occur at present. The preservation of the near-shore OFG body was thus likely enhanced by its shallow occurrence and, accordingly, a shorter duration of the salinization process in comparison to deeper areas. The sub-seafloor geology thus plays a key role in OFG evolution. The preservation of OFG in low permeability units is similar to what has been reported by Lofi et al. (2013) using borehole information from a siliciclastic margin.

At depths >300 m below sea-level, all resistivity models show a resistive formation (5-30 Ωm) labelled as either GL or LCL. CSEM inversion can detect this resistivity increase with depth but sensitivity is low. Yet, it is seen in all models and is considered a robust feature showing resistivities that exceed the core sample resistivity analysis by as much as one order of magnitude. However, if this resistivity increase is also indicative of pore fluid freshening at depth remains unanswered. LCL porosities as low as 0.02 are reported in literature, which provide an alternative explanation for these anomalously high resistivities.

The implications of our study are two-fold. First, it highlights the difficulties of mapping OFG systems with geophysical techniques in shallow lithified carbonate settings in comparison to unconsolidated siliciclastic sediments. Our MCS reflection data had poor quality and penetration, hindering the development of a robust geological model. The high spatial variability in porosity within some of the limestone formations, on the other hand, can lead to resistivity anomalies that are difficult to distinguish from pore water freshening. Constraining the origin of each resistivity anomaly would either require high-quality seismic data, borehole drilling, or other ground-truthing data (e.g. evidence of freshened groundwater seepage). Secondly, our study demonstrates that near-coastal freshened groundwater can exist offshore semi-arid, carbonate coastlines. This is an important outcome in view of the widespread occurrence of similar settings in the Mediterranean Sea and beyond. However, the OFG resource potential in such lithified carbonates should be questioned if the latter has developed in conditions similar to those of the Maltese Islands. Both, extraction rates from low permeability units and sustainability of exploiting a relict groundwater system can be considered limiting factors from a resource perspective.

Conclusions

We present a marine CSEM study from a carbonate shelf targeting OFG. By combining 2D resistivity models with seismic reflection profiles, laboratory core log measurements and borehole data, we derived a lithological model for the seafloor to the NE of the Maltese Islands. Localized resistivity anomalies were found within the Upper Coralline, Globigerina, and Blue Clay formations. In view of the reported variability in porosity, the interpretation of geophysical data from UCL is characterized by a high degree of interpretation ambiguity. This, in combination with the occurrence of some of the anomalies at the seafloor and the absence of corresponding groundwater discharge leads us to attribute the anomalies to a decrease in

porosity. The resistive anomaly along line 9 is found within the more homogeneous Globigerina formation and is more likely indicative of OFG. Numerical hydrogeological modeling suggests that the geological setting along line 9 is conducive to the formation of a disconnected and relict OFG body by emplacement during sea-level lowstands and its preservation in low permeability units during ensuing sea-level rise. OFG can potentially occur offshore the Maltese Islands, as well as in similar settings with carbonate shelves and semi-arid climates. However, in view of the relict nature of the OFG and its occurrence in low permeability units, its potential as an unconventional source of potable water is likely low. This study has demonstrated that CSEM is a suitable geophysical tool for quantitatively characterizing potential OFG bodies hosted within carbonate lithologies, although difficulties related to poorly constrained offshore geological models need to be addressed.

Acknowledgements

The authors thank Eric Attias and two anonymous reviewers for their constructive comments. This project has received funding from the European Research Council (ERC) under the European Union's Horizon 2020 research and innovation program (grant agreement No 677898 (MARCAN)). We thank Kerry Key for making MARE2DEM accessible for scientific research and allowing us to extend it to the time domain. A.H. receives funding from Digital Earth and the Future Ocean Network. J.K., M.K., Z.F. and B.W. were funded by SMART. E.R. was funded by HYFREW (CNR-University of Malta). We are grateful to Infrastructure Malta for providing access to their data. We kindly acknowledge the captain, crew and scientific party of R/V Hercules for their assistance with offshore data collection and processing. We thank the Maltese authorities for permissions to carry out the marine surveys. E.R. thanks Merilisa Guerriero, who worked on the Malta samples in the Hydrogeosite Laboratory (CNR-IMAA, Italy). Data for this research are available at <http://doi.org/10.5281/zenodo.4304549>.

References

Aeshbach-Hertig, W., & Gleeson, T. (2012). Regional strategies for the accelerating global problem of groundwater depletion, *Nat. Geoscience*, 5, 853-861. <https://doi.org/10.1038/ngeo1617>.

- Archie, G.E. (1942). The electrical resistivity log as an aid in determining some reservoir characteristics. *Journal of Petroleum Technology*, 5, 1-8. <https://doi.org/10.2118/942054-G>.
- Attias, E., Thomas, D., Sherman, D., Ismail, K., & Constable, S. (2020). Marine electrical imaging reveals novel freshwater transport mechanism in Hawai'i, *Science Advances*, 6(48). <https://doi.org/10.1126/sciadv.abd4866>.
- Attias, E., Constable, S., Sherman, D., Ismail, K., Shuler, C., & Dulai, H. (2021). Marine electromagnetic imaging and volumetric estimation of freshwater plumes offshore Hawai'i. *Geophysical Research Letters*, 48, e2020GL091249. <https://doi.org/10.1029/2020GL091249>
- Bakken, T.H., Ruden, F., & Mangset, L.E. (2012). Submarine groundwater: A new concept for the supply of drinking water. *Water Resources Management*, 26, 1015-1026. <https://doi.org/10.1007/s11269-011-9806-1>
- Bakalowicz, M. & Mangion, J. (2003). The limestone aquifers of Malta: Their recharge conditions from isotope and chemical surveys, in *Hydrology of the Mediterranean and Semiarid Regions*, Proceedings of an international symposium held at Montpellier, IAHS, no. 278.
- Bakalowicz, M. (2015). Karst and karst groundwater resources in the Mediterranean, *Environ Earth Sci*, 74, (1). <https://doi.org/10.1007/s12665-015-4239-4>.
- Berndt, C., Urlaub, M., Jegen, M., Faghih, Z., Reeck, K., Franz, G., Barnscheidt, K. C., Wollatz-Vogt, M., Liebsch, J., Schramm, B., Elger, J., Kühn, M., Müller, T., Schmidt, M., Spiegel, T., Timm, H., Hinz, A. K., Sager, T., Hilbert, H. S., Rohde, L., Korbjuhn, T., Reissmann, S. & Diller, N. (2021). RV SONNE Cruise Report SO277 OMAX: Offshore Malta Aquifer Exploration, Emden (Germany) – Emden (Germany), 14.08. – 03.10.2020. GEOMAR Report, N. Ser. 057, GEOMAR Helmholtz-Zentrum für Ozeanforschung Kiel, Germany, 139 pp. https://doi.org/10.3289/GEOMAR_REP_NS_57_20.
- Bertoni, C., Lofi, J., Micallef, A. & Moe, H. (2020). Seismic reflection methods in offshore groundwater research, *Geosciences* 2020, 10, 299. <https://doi.org/10.3390/geosciences10080299>.
- Caruso, A., Cosentino, C., Pierre, C., & Sulli, A. (2011). Sea-level changes during the last 41,000 years in the outer shelf of the southern Tyrrhenian Sea: evidence from benthic foraminifera and seismostratigraphic analysis. *Quaternary International* 232, 122–131. <https://doi.org/10.1016/j.quaint.2010.07.034>

- Cassar, J. (2010). The use of limestone in a historic context - the experience of Malta, in *Limestone in the Built environment: Present-Day Challenges for the Preservation of the Past*. Geological Society, London, Special Publications, 331, 13-25. <https://doi.org/10.1133/SP331.2>.
- Cooke, A. P., Fisher, Q. J., Michie, E. A. H. & Yielding, G. (2018). Investigating the controls on fault rock distribution in normal faulted shallow burial limestone, Malta, and the implications for fluid flow, *Journal of Structural Geology*, 114, pg. 22-42. <https://doi.org/10.1016/j.jsg.2018.05.024>.
- Cronin, T.M. (2012). Rapid sea-level rise. *Quaternary Science Reviews*, 56, 11-30. <https://doi.org/10.1016/j.quascirev.2012.08.021>
- ERA - Environment and Resources Authority (2015). The 2nd Water Catchment Management Plan for the Malta Water Catchment District 2015 - 2021, Sustainable Energy and Water Conservation Unit Environment and Resources Authority.
- Evans, R. L., & Lizarralde, D. (2011). The competing impacts of geology and groundwater on electrical resistivity around Wrightsville Beach, NC. *Continental Shelf Research*, 31, 7-8, pg. 841-848. <https://doi.org/10.1016/j.csr.2011.02.008>.
- Food and Agriculture Organization (FAO) of the United Nations (2006). Malta Water Resources Review, FAO, Rome, Italy. Available online: <http://www.fao.org/3/a-a0994e.pdf> (accessed on 02 July 2020).
- Freeze, R.A., & Cherry, J.A. (1979). *Groundwater*, Prentice Hall Inc. <http://hydrogeologistswithoutborders.org/wordpress/1979-english/>
- Fusi, N., & Castellanza, R. (2019). Permeability test and porous system analysis on Malta calcarenites and New Zealand Clay. University of Milano Bicocca, Report for MARCAN project.
- Gatt, P. A. (2012). Carbonate facies, depositional sequences and tectonostratigraphy of the paleogene Malta platform, Durham Theses, Durham University, <http://etheses.dur.ac.uk/4425/>.
- Galdies, C. (2013). The Climate of Malta: Statistics, Trends and Analyses 1951 - 2010. National Statistics Office, Valletta, Malta.
- Glover, P. (2016). Archie's Law - A reappraisal, *Solid Earth and Discussions*, 7(4), 1157-1169. <https://doi.org/10.5194/se-2016-47>.
- Goldscheider, N., Chen, Z., Auler, A., Bakalowicz, M., Broda, S., Drew, D., Hartmann, J., Jiang, G., Moosdorf, N., Stevanovic, Z., & Veni, G. (2020). Global distribution of

- carbonate rocks and karst water resources, *Hydrogeology*, 28, 1661-1677.
<https://doi.org/10.1007/s10040-020-02139-5>.
- Gustafson, C., Key, K., & Evans, R. (2019). Aquifer systems extending far offshore on the U.S. Atlantic Margin, *Scientific Reports*, 9, 1, 8709. <https://doi.org/10.1038/s41598-019-44611-7>
- Harrar, W.G., Williams, A.T., Barker, J.A., & Camp, M.V. (2001). Modelling scenarios for the emplacement of palaeowaters on aquifer systems. In: W.M. Edmunds, C.J. Milne (Eds.), *Palaeowaters in Coastal Europe: Evolution of Groundwater Since the Late Pleistocene*. Geological Society of London, London, pp. 213-229.
<https://doi.org/10.1144/GSL.SP.2001.189.01.13>
- Haroon, A., Lippert, K., Mogilatov, M., & Tezkan, B. (2018a). First application of the marine differential electric dipole for groundwater investigations: A case study from Bat Yam, Israel, *Geophysics*, 83, 2, pg. B59-B76. <https://doi.org/10.1190/GEO2017-0162.1>.
- Haroon, A., Hölz, S., Weymer, B. A., Tezkan, B., & Jegen, M. (2018b). Calculating Time-Domain Controlled Source Electromagnetic Signals with MARE2DEM, in *Conference Proceedings of 3rd Applied Shallow Marine Geophysics Conference*, 2018, pg. 1-5.
<https://doi.org/10.3997/2214-4609.201802663>.
- Haroon, A., Swidinsky, A., Hölz, S., Jegen, M., & Tezkan, B. (2020). Step-on versus step-off signals in time-domain controlled source electromagnetic methods using a grounded electric dipole, *Geophysical Prospecting*, 68(9), 2825-2844. <https://doi.org/10.1111/1365-2478.13016>.
- Henri, C.V., Harter, T., & Diamantopoulos, E. (2019). On the Conceptual Complexity of Non-Point Source Management: Impact of Spatial Variability. *Hydrology and Earth System Sciences*. <https://doi.org/10.5194/hess-2019-499>.
- Illies, J. H. (1981). Graben formation - The Maltese Islands, a case study, *Tectonophysics*, 73, 151-168. [https://doi.org/10.1016/0040-1951\(81\)90182-7](https://doi.org/10.1016/0040-1951(81)90182-7)
- Key, K. (2016). MARE2DEM: a 2-D inversion code for controlled-source electromagnetic and magnetotelluric data, *GJI*, 207, 571-588. <https://doi.org/10.1093/gji/ggw290>.
- Kuang, X., Jiao, J.J., Zheng, C., Cherry, J.A., & Li, H. (2020). A review of specific storage in aquifers. *Journal of Hydrology* 581. <https://doi.org/10.1016/j.jhydrol.2019.124383>.
- Lambeck, K., Antonioli, F., Anzidei, M., Ferranti, L., Leoni, G., Scicchitano, G. & Silenzi, S. (2011). Sea level change along the Italian coasts during Holocene and prediction for the future. *Quaternary International* 232, 250-257.
<https://doi.org/10.1016/j.quaint.2010.04.026>

- Langevin, C.D., Thorne Jr., D.T., Dausman, A.M., Sukop, M.C., & Guo, W. (2008). SEAWAT version 4: a computer program for simulation of multi-species solute and heat transport. US Geological Survey Techniques and Methods Book. 6 (chapter A22). <https://doi.org/10.3133/tm6A22>
- Laugié, M., Michel, J., Pohl, A., Poli, E., & Borgomano, J. (2019). Global distribution of modern shallow-water marine carbonate factories: a spatial model based on environmental parameters. *Sci Rep* 9, 16432. <https://doi.org/10.1038/s41598-019-52821-2>.
- Lofi, J., Pezard, P., Bouchette, F., Raynal, O., Sabatier, P., Denchik, N., Levannier, A., Dezileau, L., & Certain, R. (2013), Integrated Onshore- Offshore Investigation of a Mediterranean Layered Coastal Aquifer. *Groundwater*, 51, 550-561. <https://doi.org/10.1111/j.1745-6584.2012.01011.x>
- Margat, J. (1998). Les eaux souterraines dans le bassin méditerranéen. Ressources et utilisations. Documents BRGM 282. BRGM, Orléans, France. ISBN: 2715908768
- Meisler, H., Leahy, P.P., & Knobel, L.L. (1984). Effect of Eustatic Sea-Level Changes on Saltwater-Freshwater relations in the Northern Atlantic coastal plain, U.S. Geological Survey. <https://doi.org/10.3133/wsp2255>
- Micallef, A., Foglini, F., Le Bas, T., Angeletti, L., Maselli, V., Pasuto, A., & Taviani, M. (2013). The submerged paleolandscape of the Maltese Islands: Morphology, evolution and relation to Quaternary environmental change, *Marine Geology*, 335, pg. 129-147. <https://doi.org/10.1016/j.margeo.2012.10.017>.
- Micallef, A., Berndt, C., Berndt, J., Jegen, M., Schwalenberg, K., Wollatz-Vogt, M., Haroon, A., Garzia, X., Faghih, Z., Spatola, D., Worzewski, T., Zerbst, J. & MARCAN, University of Malta, BGR, etc, GEOMAR (2019) Cruise Report RV Hercules [MARCAN Malta 2018], Valletta-Valletta, 1.-10.10.2018, MARCAN Project. University of Malta, Malta, 37 pp. <http://oceanrep.geomar.de/id/eprint/49319>
- Micallef, A., Person, M., Haroon, A., Weymer, B. A., Jegen, M., Schwalenberg, K., Faghih, Z., Duan, S., Cohen, D., Mountjoy, J. J., Woelz, S., Gable, C. W., Avers, T., & Tiwari, A. K. (2020). 3D characterisation and quantification of an offshore freshened groundwater system in the Canterbury Bight, *Nature Communications*, 11, 1372. <https://doi.org/10.1038/s41467-020-1470-7>.
- Micallef, A., Person, M., Berndt, C., Bertoni, C., Cohen, D., Dugan, B., Evans, R., Haroon, A., Hensen, C., Jegen, M., Key, K., Kooi, H., Liebetrau, V., Lofi, J., Mailloux, B. J., Martin-Nagle, R., Michael, H.A., Mueller, T., Schmidt, M., Schwalenberg, K., Trembath-Reichert, E., Weymer, B., Zhang, Y., & Thomas, A. T. (2021). Offshore freshened

- groundwater in continental margins, *Reviews of Geophysics*.
<https://doi.org/10.1029/2020RG000706>.
- Michael, H. A., Scott, K. C., Koneshloo, M., Yu, X., Khan, M. R., & Li, K. (2016), Geologic influence on groundwater salinity drives large seawater circulation through the continental shelf, *Geophys. Res. Lett.*, 43, 10,782– 10,791. <https://doi.org/10.1002/2016GL070863>.
- Michael, H. A., Post, V. E. A., Wilson, A. M., & Werner, A. D. (2017). Science, society, and the coastal groundwater squeeze, *Water Resources Research*, 53, 4, pg. 2610-2617. <https://doi.org/10.1002/2017WR020851>.
- Oil Exploration Directorate (OED) (1993). Geological map of the Maltese Islands. Office of the Prime Minister, Valletta. Shapefiles downloaded from <https://continentalshelf.gov.mt>
- Paldor, A., Katz, O., Aharonov, E., Weinstein, Y., Roditi-Elasar, M., Lazar, A., & Lazar, B. (2020). Deep Submarine Groundwater Discharge Evidence from Achziv Submarine Canyon at the Exposure of the Judea Group Confined Aquifer, Eastern Mediterranean, *JGR: Oceans*, 125, 1, <https://doi.org/10.1029/2019JC015435>.
- Pedley, H. M., House, M. R., & Waugh, B. (1976). The Geology of Malta and Gozo, *Proc. Geol. Ass.*, 87, 3, 325-341.
- Person, M., Dugan, B., Swenson, J. B., Urbano, L., Stott, C., Taylor, J., & Willett, M. (2003). Pleistocene hydrogeology of the Atlantic continental shelf, New England. *Geol. Soc. Am. Bull.* 115, 1324–1343.
- Post, V. E. A., Groen, J., Kooi, H., Person, M., Ge, S. & Mike Edmunds, W. (2013). Offshore fresh groundwater reserves as a global phenomenon, *Nature*, 504, pg. 71-78. <https://doi.org/10.1038/nature12858>.
- Richey, A. S., Thomas, B. F., Lo, M. L., Reager, J. T., Famiglietti, J. S., Voss, K., Swenson, S., & Rodell, M. (2015). Quantifying renewable groundwater stress with GRACE, *Water Resource Research*, 51, 7. <https://doi.org/10.1002/2015WR017349>
- Sapiano, M., Schembri, M., Debattista, H., & Theuma, N. (2017a). Integrating numerical models in river basin management plans: The Freewat project, *Water Resources Management*, 220. <https://doi.org/10.2495/WRM170221>.
- Sapiano, M., Schembri, M., & Debattista, H. (2017b). Optimising the management of the Gozo mean sea-level aquifer (Malta), in *The Energy & Water Agency*, Pisa, 12th July 2017.
- Schulze-Makuch, D. (2005). Longitudinal dispersivity data and implications for scaling behaviour, *Groundwater*, 43, (3), pg. 443-456. <https://doi.org/10.1111/j.1745-6584.2005.0051.x>.

- Schwalenberg, K., Rippe, D., Koch, S., & Scholl, C. (2017). Marine-controlled source electromagnetic study of methane seeps and gas hydrates at Opouawe Bank, Hikurangi Margin, New Zealand. *J. Geophys. Res. Solid Earth*, 122, 3334-3350. <https://doi.org/10.1002/2016JB013702>.
- Schön, J. H. (2004). *Physical Properties of Rocks: Fundamentals and Principles of Petrophysics*. In: Helbig K and Treitel S (eds.) vol. 18 Amsterdam, The Netherlands: Elsevier, ISBN: 008044346X, 2004.
- Stuart, M. E., Maurice, L., Heaton, T. H. E., Sapiano, M., Micallef Sultana, M., Gooddy, D. C., & Chilton, P. J. (2010). Groundwater residence time and movement in the Maltese islands - a geochemical approach, *Applied Geochemistry*, 25, 5, pg. 609 – 620. <https://doi.org/10.1016/j.apgeochem.2009.12.010>.
- Verweij, H., Vis, G.J., & Imborechts, E. (2016). Spatial variation in porosity and permeability of the Rupel Clay Member in the Netherlands, *Netherlands Journal of Geosciences*, 95(3), 253–268. <https://doi.org/10.1017/njg.2016.28>
- Zheng, C. (1990). MT3D; A modular three-dimensional transport model for simulation of advection, dispersion and chemical reactions of contaminants in groundwater systems. Report, Rockville, Maryland: S.S. Papadopoulos & Associates. https://hydro.geo.ua.edu/mt3d/Mt3d_1990.pdf

Figure list

Figure 1: (a) Geological map of the Maltese Islands with the main formations highlighted by the colors shown in the legend (OED, 1993). Main faults illustrated by black lines whereas yellow and orange lines located to the east of the archipelago depict the CSEM and seismic reflection profiles collected in October 2018, respectively. The white contour marks the paleo shoreline at 20 ka before present. Locations of where core samples were retrieved and the borehole BH3 are illustrated by blue and pink circles, respectively. (b) Close-up image of line 8 located east of Gozo. (c) Close-up image of lines 2, 5, and 6. The red shaded areas mark box canyons. Island topography is displayed by the corresponding color scale in panels (b) and (c).

Figure 2: CSEM resistivity overlays with geological units derived using seismic reflection (cf. Figure S14 of SI) and borehole (BH3) data. Lithological units are illustrated and labelled by the pale color scheme shown in the legend, whereas resistivity models adhere to the color scale.

Location of each CSEM line is schematically illustrated on the top right. (a-e) Resistivity models overlying the lithological interpretation for each CSEM line. Triangles mark the stationary waypoints of the transmitter dipole. (b) Lithological classification of borehole BH3 is displayed as an extension of line 2 towards the southwest. ROV imagery was taken at the base of the escarpment along the extension of line 2 towards the northeast. The inserted picture shows the retrieved LCL sample.

Figure 3: Illustrations to aid the interpretation of the resistivity models shown in Figure 2. (a) Resistivity relationship for varying pore fluid salinity and matrix porosity based on Archie's equations (Archie, 1942). The white lines depict specific resistivity contours. Lower panels show resistivity as a function of porosity and cementation exponent (m) for (left) seawater (38 PSU) and (right) freshened water (10 PSU). (b) Salinity model in PSU at present state derived by hydrogeological modeling for an anisotropy factor of 100 using offshore geology and past sea-level lowstands. Note that the salinity was converted from g/l to PSU assuming a density of 1000 g/l. Light colors at >3000 m depict the possible OFG body hosted within GL and BC. (c) Resistivity model along line 9 for qualitative comparison to the salinity model displayed in (b). Note that the x-axis of (c) was aligned so that 0 m represents the present-day coastline and is therefore shifted in comparison to Figure 2a.

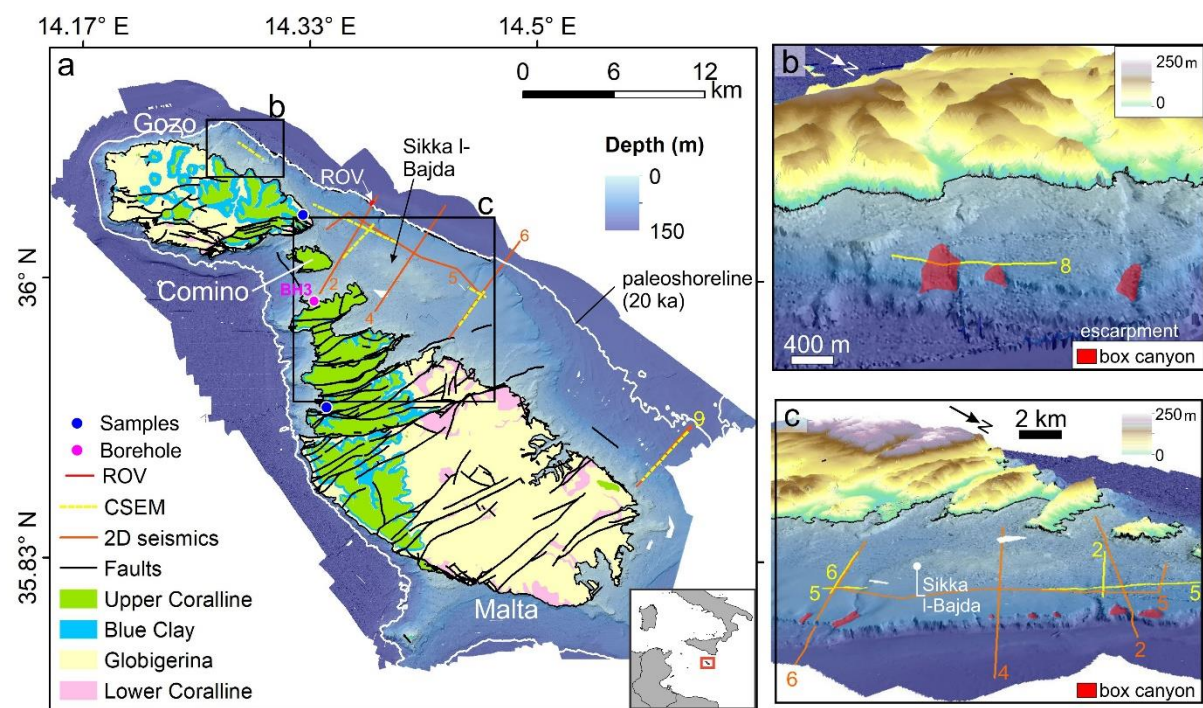


Figure 1

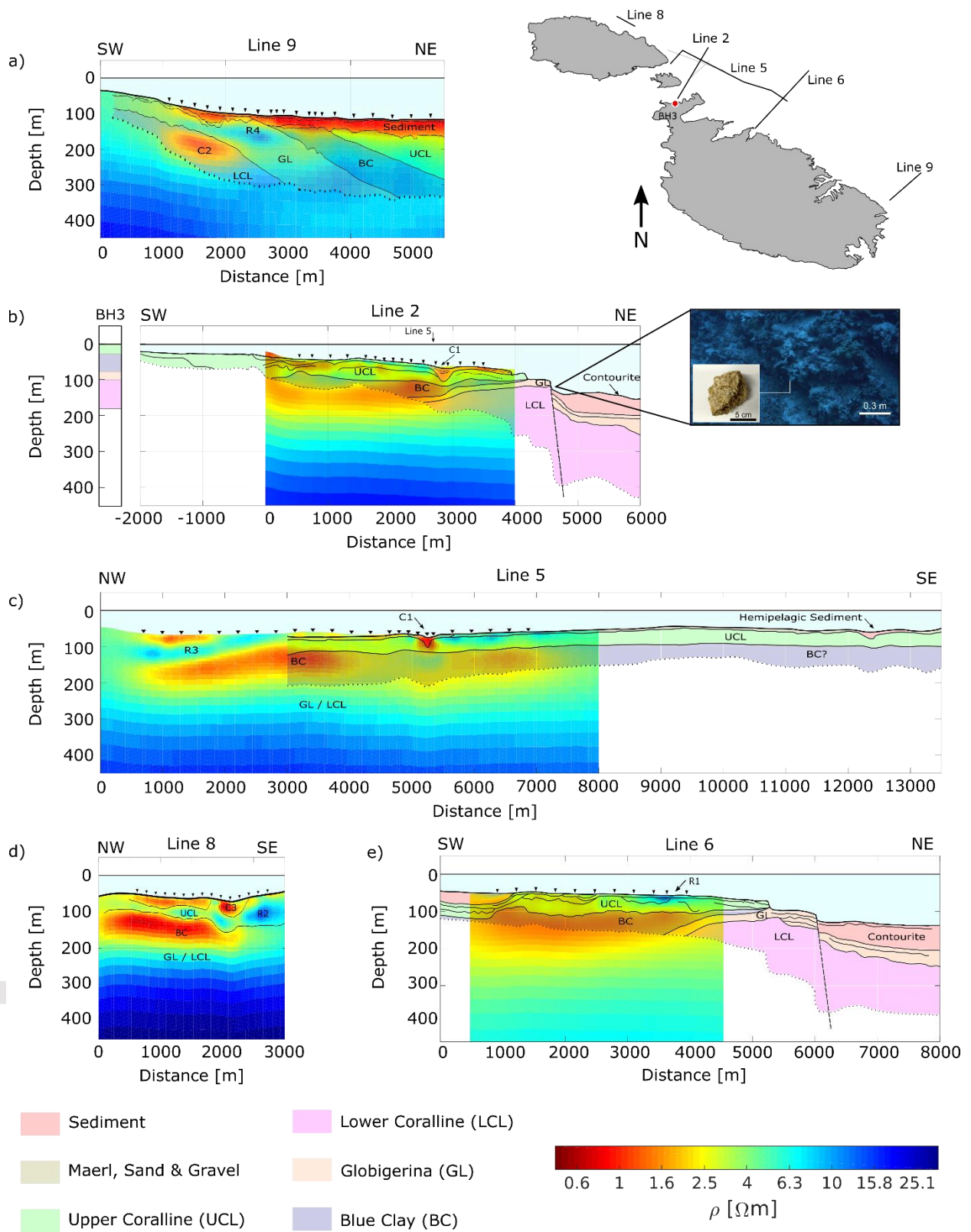


Figure 2

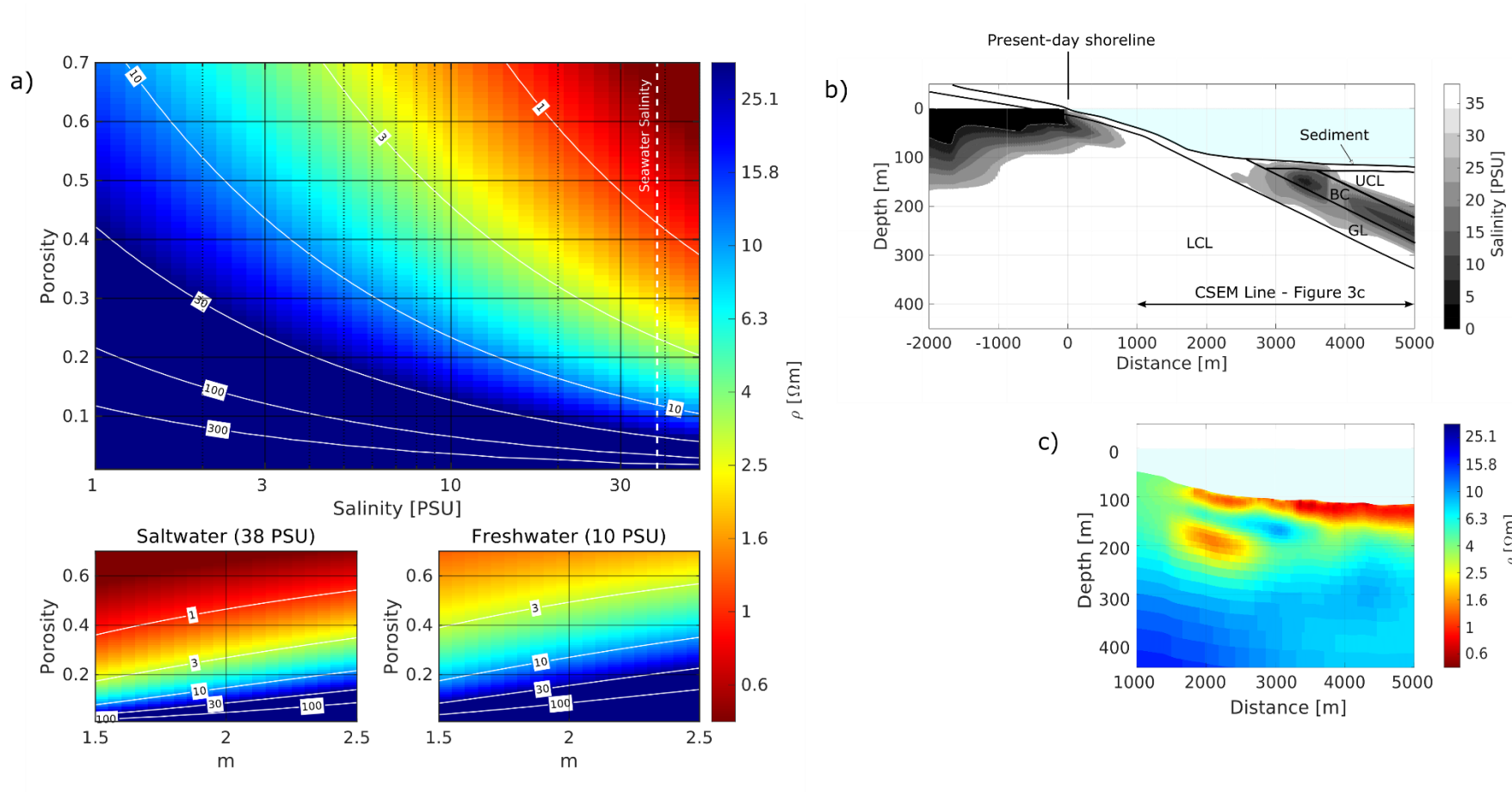


Figure 3

Formation	Member	Porosity		Hydraulic Conductivity (m/s)		P-Wave Velocity (m/s)		Thickness at BH3 (m)	Density (g/cm ³)	Resistivity (Ωm) seawater saturated
		Literature ^{1,2,3}	Measured	Literature ^{4,5,6}	Measured					
Upper Coralline	Tal-Pitkal (UCL-T)	0.02 - 0.45	-	10 ⁻⁵ - 10 ⁻⁸	-	2741	20.5	2.60	-	
	Mtarfa (UCL-M)		0.3		5.0 x 10 ⁻⁷			1.77	1.96	
Blue Clay	BC	0.35	-	10 ⁻⁸	5.90 x 10 ⁻¹¹	1700	52	1.87	-	
Globigerina (GL)	Upper (UGL)	0.24 - 0.41	0.36	8 - 9.95 x 10 ⁻⁶	4.0 x 10 ⁻⁹	2113	2066	8	1.53	2.27
	Middle (MGL)		0.29		8.30 x 10 ⁻¹⁰	1993		11	1.65	2.38
	Lower (LGL)		0.27		1.68 x 10 ⁻⁸	2335		6	1.79	2.68
Lower Coralline (LCL)	Xlendi (LCL-X)	0.02 - 0.3	-	0.2 - 9.95 x 10 ⁻⁴	-	2957	79	2.54	-	
	Attard (LCL-A)	0.02 - 0.28	0.19		7.28 x 10 ⁻⁸			2.09	4.43	

1: Stuart et al (2010); 2: Cassar (2010); 3: Cooke et al. (2018); 4: Bakalowicz & Mangion (2003) 5: Sapiano et al. (2017a,b) 6: ERA (2015).

